Site-selective spectroscopic study on the dynamics of exciton hopping in an array of inhomogeneously broadened quantum dots

Jun Miyazaki*
Advanced Ultrafast Laser Research Center, University of Electro-Communications, Chofugaoka 1-5-1, Chofu, Tokyo 182-8585, Japan

Shuichi Kinoshita
Graduate School of Frontier Biosciences, Osaka University, Yamadaoka 1-3, Suita, Osaka 565-0871, Japan
(Received 16 May 2012; revised manuscript received 12 June 2012; published 5 July 2012)

We investigate the dynamics of exciton hopping in a CdSe/ZnS quantum dot (QD) array composed of an inhomogeneously broadened ensemble. Time- and spectrally resolved fluorescence intensities are measured by varying the excitation photon energy at the absorption edge. This method allows us to observe fluorescence from only the subdistribution of the QD ensemble, thereby allowing the dynamics of exciton hopping, which depends on the initial (donor) exciton energy, to be elucidated. Experimental results along with numerical calculations using a model of a coupled QD array show that when high-energy QDs are selectively excited, exciton energy transfer occurs repeatedly to a site of low energy, leading to a large exciton hopping length. In contrast, when the low-energy end of the QD ensemble is excited, the exciton tends to be trapped in the initial QD. Furthermore, from the analysis of the decay time of fluorescence intensities, it is suggested that there are dark QDs associated with the defect and/or off state of blinking QDs in the ensemble and energy transfer to such a site is mainly followed by quenching.

DOI: 10.1103/PhysRevB.86.035303 PACS number(s): 78.67.Hc, 81.07.Ta, 78.47.jd, 66.30.Ma

I. INTRODUCTION

The optical properties of coupled semiconductor quantum dots (QDs) have attracted considerable attention over the past decade because of their applicability to the realization of optoelectric devices such as quantum logic gates[1–3] and their potential use in photovoltaic cells.[4,5] Excitation energy transfer from interdot electric coupling plays an essential role in such systems, and this process is considered to strongly influence their operational parameters. Several experimental studies have shown that, in spatially separated QDs, energy transfer occurs from a small to a large QD, corresponding to a high-to-low excitonic energy state, which is directly reflected in the fluorescence intensity in both the temporal and the spectral domains.[6–20] For example, in a mixture of two differently sized QD ensembles, the ratio of the fluorescence intensity of the donor to that of the acceptor decreases with time because of energy transfer.

In a monodispersed QD ensemble, a fluorescence dynamic red shift appears because spectral broadening arises from the size distribution of individual QDs in the ensemble (inhomogeneous broadening), and energy transfer occurs preferably to a site of low energy.[7,9,11,16,18,19] A similar process can be seen in inhomogeneously broadened conjugated polymers and light-harvesting antennae.[21,22] In the case of photovoltaic cells, this process is crucial to device performance since the exciton transport (hopping) length is a critical parameter in the conversion efficiency.

More recently, we have studied the dynamics of exciton hopping in an array of inhomogeneously broadened CdSe/ZnS QDs by measuring time- and spectrally resolved fluorescence intensities.[23] It has been shown that the exciton dynamics depends on temperature. At low temperatures, excitons tend to be trapped in a local low-energy site. However, the hopping probability increases as the temperature increases. It has been also suggested that the decrease in decay time of the QD array is attributed to exciton hopping to a dark QD associated with the defect and/or off state of the blinking QD. In the presence of dark QDs, an exciton is considered to exhibit fast nonradiative decay when it reaches the dark QD. This scheme is similar to the photoprotection mechanism in a light-harvesting system, where molecules such as carotenoids dissipate excess energy as heat to avoid the generation of toxic photo-oxidative intermediates.[24–26] Further, this scheme is crucial for both organic and nanocrystal light-emitting diodes since it controls how excitons are quenched by impurities or other quenching centers.[27,28]

However, in the previous studies, the excitation photon energy is usually set much higher than the absorption edge so that all QDs will contribute to the measured fluorescence, irrespective of the energy level. In fact, the exciton dynamics depends on the initial exciton energy, as is evident from the fact that excitation transfers occur preferably from a high- to a low-energy state. Thus, to elucidate the dynamics of exciton hopping, the effect of the initial exciton energy should be examined.

In this study, we have measured time- and spectrally resolved fluorescence intensities by means of site-selective spectroscopy at both room and low temperature. Thus far, the method of site-selective excitation has been employed to study energy transfer in several inhomogeneous systems such as europium-doped crystals, conjugated polymer guest-host systems, and photosynthetic bacteria.[29–32] This approach gives insight into the spectral characteristics of individual molecules and their distributions as well as enabling us to identify the dynamics of energy transfer, which depend on the initial (donor) exciton energy. In the present study, we have performed a fluorescence measurement by varying the excitation photon energy around the absorption edge. This method allows us to observe the fluorescence only from

the subdistribution of the QD ensemble, and thereby, the dependence of the dynamics of exciton hopping on the initial (donor) exciton energy level can be elucidated.

II. MATERIALS AND METHODS

The CdSe/ZnS core/shell nanocrystals capped with octadecylamine purchased from NN Labs, Inc., have a fluorescence peak at 2.14 eV (580 nm) and a fluorescence quantum yield of approximately 50%. QD arrays were prepared by dropping the sample in toluene on a quartz plate under an argon atmosphere. The sample was then dried in vacuum for several hours to evaporate the solvent. From transmission electron microscopy (TEM) measurements, we confirmed that the QD ensemble forms a two-dimensional (2D) close-packed network with hexagonal order. The average diameter and interdot distance of the QD array were found to be 5.2 and 7.9 nm, respectively.

An optical parametric amplifier pumped by a 1-kHz regenerative Ti:sapphire laser was employed as the light source. The excitation photon energy was tunable from 2.0 to 3.1 eV. A grating pair and a slit were employed to reduce the bandwidth of the pulse to less than 2 nm full width at half-maximum (FWHM). The power density of the excitation pulse was sufficiently weak (20 nJ/cm^2) to avoid multiexciton generation in a single QD. We ensure that the increase and decrease in the excitation intensity had no effect on the spectral and temporal fluorescence profile.

A streak camera (Hamamatsu C4780) and a monochrometer (Chromex 250is) were employed to obtain time- and spectrally resolved fluorescence intensities with a wavelength resolution of 0.9 nm. Fluorescence measurements were performed for two streak speeds, 0.01 and 0.1 ns/pixel. The corresponding measuring time ranges were 5 and 50 ns, and the typical time resolutions were 0.05 and 0.6 ns, respectively. A polarizer and a polarization scrambler were placed between the sample and the monochromator, and the polarization was set to be perpendicular to that of the excitation laser light to reduce the contamination from the excitation light. Absorption spectra of the QD samples were measured using a spectrophotometer equipped with an integrating sphere (JASCO V-670). The sample temperature was controlled either by a transparent glass dewar or by a liquid nitrogen cryostat system (Janis Research VNF-100) over a temperature range of 80 K to room temperature (294 K).

III. EXPERIMENTAL RESULTS

A. Edge excitation red shift

We first measured the absorption and fluorescence spectra of QD dispersion. The measured spectra are considerably broadened owing to the size distribution of the QD ensemble. This can be directly confirmed by observing the edge excitation red shift (EERS) by varying the excitation photon energy E_{exc} at the absorption edge. Figure 1(a) shows the fluorescence spectra at various E_{exc} at room temperature. The absorption spectrum of QD dispersion is also shown. When E_{exc} is varied below 2.27 eV, the average fluorescence photon energy E_{fluo} (center of spectral mass) depends linearly on it with a slope of 0.46, as shown in Fig. 1(c). When E_{exc} is reduced below 2.10 eV, E_{fluo} becomes even higher than E_{exc}. These results clearly show the selective excitation of larger QDs in the ensemble. On the other hand, when E_{exc} is from 2.20 to ~2.27 eV, small QDs are considered to be excited preferentially because E_{exc} is larger than the first absorption peak at 2.20 eV. According to the analysis of EERS, the inhomogeneous distribution and the homogeneous line width are estimated from the value of the slope to be 33 and 36 meV, respectively.[23] The widths obtained are used for parameters in the numerical calculations presented later.

When E_{exc} is at the absorption edge, an exciton is considered to be mainly formed through direct excitation to the lowest-energy exciton state. In contrast, when E_{exc} is above ~2.28 eV, a higher energy exciton is formed, which is followed by the relaxation to the lowest-energy exciton state, as implied from the shape of the absorption spectrum. Therefore, as E_{exc} increases above ~2.28 eV, the fluorescence from large QDs excited through this process begins to dominate over the fluorescence from small QDs excited directly to the lowest energy exciton state. This explains the decrease in E_{fluo} as well as the deviation of the proportional relation between E_{exc} and E_{fluo}. In fact, when E_{exc} is at 2.34 eV, two peaks appear, at 2.11 and 2.25 eV, in the fluorescence spectrum, which are assigned to the fluorescence from large QDs excited

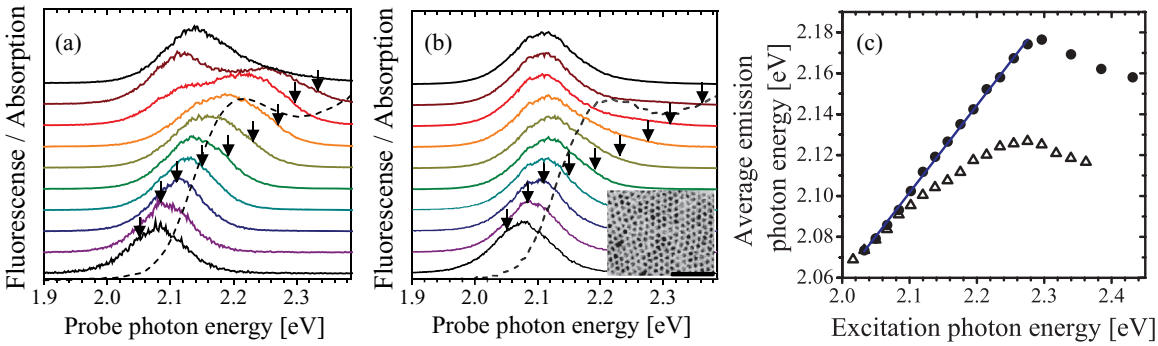

FIG. 1. (Color online) Series of (temporally integrated) fluorescence spectra of (a) QD dispersion and (b) QD arrays at various excitation photon energies E_{exc}. The absorption spectra are shown as a dashed line. Arrows show the position of E_{exc}. The fluorescence spectra at the top of (a) and (b) are obtained when E_{exc} is at 3.1 eV. The inset in (b) shows a TEM image of a QD forming a two-dimensional close-packed network with hexagonal order. Scale bar: 50 nm. (c) Average fluorescence photon energy E_{fluo} of the QD dispersion (filled circles) and the QD array (open triangles) as a function of E_{exc}. The solid line, with a slope of 0.46, corresponds to a linear fit of the points in the low-energy region.

through higher energy exciton states and the fluorescence from small QDs excited directly to the lowest energy exciton state, respectively. When E_{exc} is much higher than the absorption edge, E_{fluo} remains almost constant at 2.15 eV. In this case, all QDs are considered to be excited irrespective of their size through high-energy levels.

Figure 1(b) shows absorption and (temporally integrated) fluorescence spectra of the QD array. The inset shows a TEM image of the QD array. The absorption spectrum of the QD array is nearly the same as that of QD dispersion. In contrast, the fluorescence spectra are red-shifted, especially for large E_{exc}. Figure 1(c) shows that the E_{fluo} of the QD array is nearly the same as that of the QD disperision for small E_{exc}. However, as E_{exc} is increased, the E_{fluo} of the QD array becomes smaller than that of the QD dispersion. These fluorescence properties are further characterized by the time-resolved spectra presented in the following section.

B. Time-resolved fluorescence spectrum

In the previous work, time- and spectrally resolved fluorescence intensities of QD arrays were measured at $E_{exc} = 2.76$ eV, so that all the QDs are assumed to be excited irrespective of their size.[23] The fluorescence decay time of the QD array in the low-energy region of the fluorescence spectrum was found to be longer than that in the high-energy region, which leads to a dynamic red shift of the fluorescence spectrum. This is direct evidence of energy transfer from a small to a large QD in the ensemble. Since these fluorescence profiles should strongly depend on E_{exc}, we have constructed time-resolved fluorescence spectra for various excitation energies.

Figures 2 and 3 show the time and spectrally resolved fluorescence intensities and the time traces of E_{fluo}, respectively, at various values of E_{exc}. In Fig. 3, the data for two streak speeds are connected at 4 ns. The initial value of E_{fluo} depends on E_{exc} in a manner similar to that described in the preceding section. It is evident that the fluorescence spectrum of the QD array for $E_{exc} = 2.25$ eV is red-shifted with time, as shown at the top in Fig. 2. The rate of the energy shift decreases with time. In addition, the fluorescence width is found to decrease with time. It is noteworthy that the magnitude of the red shift decreases as E_{exc} decreases. As shown in Fig. 3, a unique feature is that, when E_{exc} is above ~2.16 eV, the time traces of E_{fluo} approach a nearly constant value after 20 ns. As E_{exc} is reduced in the range below ~2.12 eV, E_{fluo} decreases after 20 ns, although it is difficult to conclude whether the time traces of E_{fluo} converge in the long-time limit as the intensities decay with time. When E_{exc} is further reduced, to 2.05 eV, the initial stage of E_{fluo} increases slightly (from 2.074 at 0.5 ns to 2.078 eV at 5 ns). In contrast, the time trace of E_{fluo} of the QD dispersion is nearly constant with time as shown in Fig. 3.

We also performed site-selective studies at low temperature (80 K), because the spectral width decreases to ~23 meV, so that both the site selectivity and the effect of inhomogeneities are expected to be enhanced.[23] Figures 4 and 5 show the time- and spectrally resolved fluorescence intensities and the time traces of E_{fluo}, respectively, at 80 K. The peak positions of the absorption and the initial fluorescence spectra depend on the temperature, owing to lattice contraction with decreasing

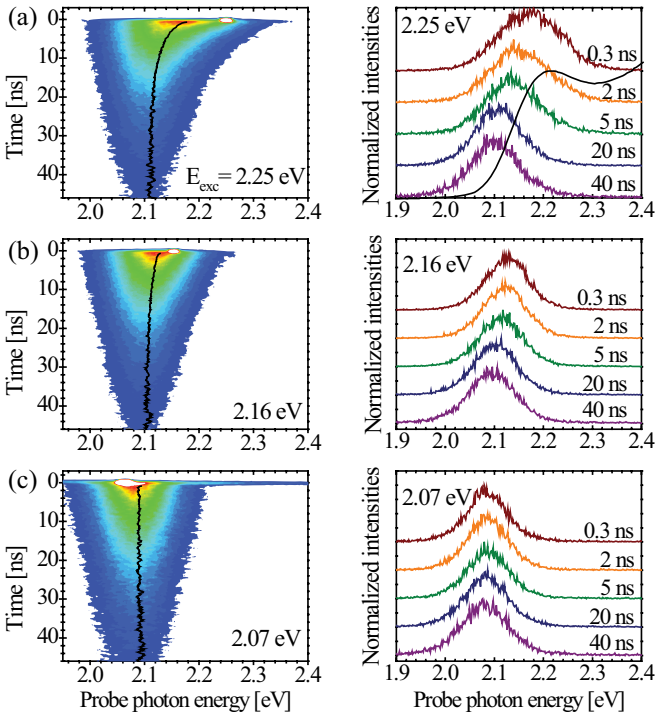

FIG. 2. (Color online) Left: Time- and spectrally resolved fluorescence intensities with various excitation energies E_{exc} at room temperature (294 K). Black lines show time traces of the average fluorescence photon energies. E_{exc} is set at (a) 2.25 eV, (b) 2.16 eV, and (c) 2.07 eV. Contamination of the excitation light appears at the initial stage. Right: Time-resolved fluorescence spectra obtained at 0.3, 2, 5, 20, and 40 ns, where the intensities are normalized for clarity. The absorption spectrum of the QD dispersion at room temperature is also shown at the top; the first absorption peak is at 2.20 eV.

temperature, which is explainable using Varshni's empirical equation $E_{fluo,a} = E^0_{fluo,a} - \alpha T^2/(\beta + T)$ with parameters of $E^0_{fluo} = 2.22$, $E^0_a = 2.27$ eV, $\alpha = 4.19 \times 10^{-4}$ eV/K, and $\beta = 230$ K.[23] When E_{exc} is much higher than the absorption edge, the magnitude of the red shift becomes large with a decrease in temperature because an exciton is preferentially trapped in a low-energy site.[23] As E_{exc} decreases, the magnitude of this red

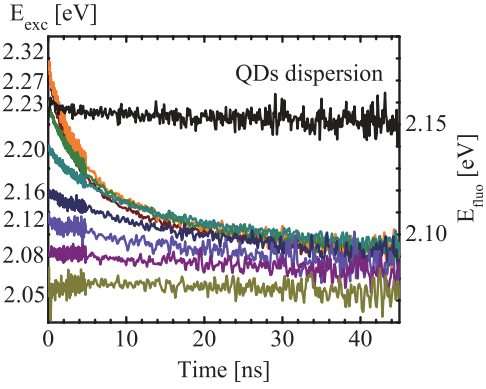

FIG. 3. (Color online) Time traces of the average fluorescence photon energy E_{fluo} of the QD array at various values of excitation photon energies E_{exc}. A time trace of E_{fluo} of the QD dispersion at $E_{exc} = 2.58$ eV is also shown for comparison.

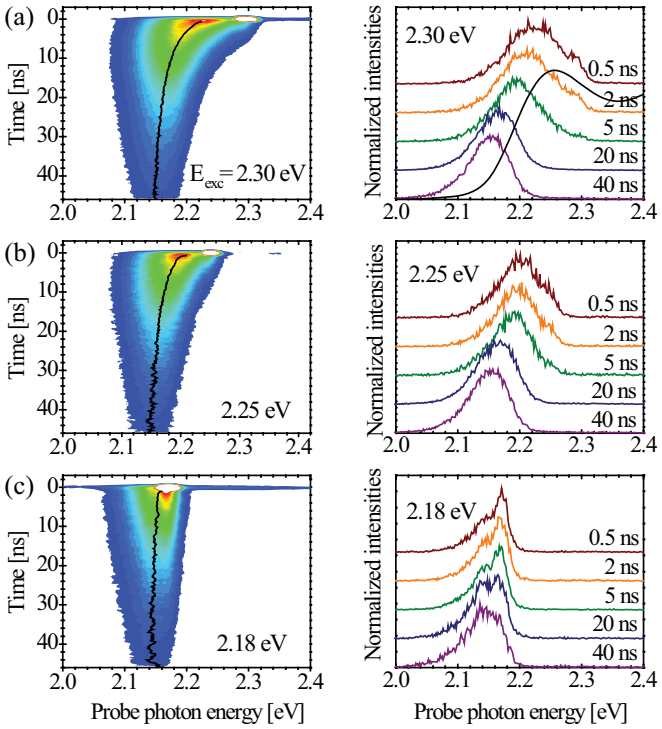

FIG. 4. (Color online) Left: Time- and spectrally resolved fluorescence intensities at a low temperature (80 K). Right: Time-resolved fluorescence spectra obtained at 0.5, 2, 5, 20, and 40 ns. Excitation photon energy E_{exc} is set at (a) 2.30 eV, (b) 2.25 eV, and (c) 2.18 eV. The absorption spectrum of QD dispersion at 100 K is also shown at the top; the first absorption peak is at 2.26 eV.

shift decreases as in the case at room temperature. When E_{exc} is reduced to 2.18 eV, a phonon side band seems to appear in the low-energy region of the fluorescence spectrum, as shown at the bottom right in Fig 4. Figure 5 shows that the time trace of E_{fluo} monotonically decreases or remains constant when E_{exc} is decreased to 2.16 eV.

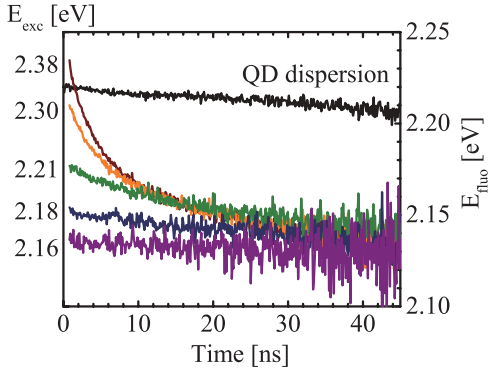

FIG. 5. (Color online) Time traces of the average fluorescence photon energy E_{fluo} of the QD array with various excitation photon energies E_{exc} at 80 K. The time trace of E_{fluo} of QD dispersion is also shown.

C. Fluorescence decay time

It has been shown that the fluorescence decay time of a QD array is generally shorter than that of QD dispersion and depends strongly on temperature.[23] In the previous work, we considered a dark QD in view of the fact that nonradiative carrier loss is different for each QD and an individual QD usually exhibits intermittent switching between the dark (off) and the bright (on) state due to defects or excess charges on the QD surface.[33–39] Since this blinking is observed on a much longer time scale than the radiative decay time, an off-state QD can be regarded as a dark QD, and exciton energy transfer to such dark QDs should mainly result in quenching, leading to a decrease in the fluorescence decay time. If the measured decrease in the fluorescence decay time is attributed to this exciton behavior, the decay time is expected to depend on E_{exc}.

We have examined the temporal behavior of the fluorescence intensity by varying E_{exc}. Figures 6(a) and 6(b) show the spectrally integrated fluorescence intensities with various values of E_{exc} at room temperature and 80 K, respectively. The decay curves are normalized at 45 ns because considerable contamination of the excitation light appears at the initial stage. It is evident that the fluorescence decay curve strongly depends on E_{exc}. The fluorescence decay time of the QD array as a function of E_{exc} is shown in Fig. 6(c). Since the decay curves are nonexponential, the fluorescence decay time τ is obtained from the relation

$$\tau = \int_{t_0}^{t_1} tI(t)dt \Big/ \int_{t_0}^{t_1} I(t)dt, \tag{1}$$

where $I(t)$ is the spectrally integrated fluorescence intensity. In Fig. 6(c), we set $t_0 = 0.5$ ns to exclude the initial contamination of the excitation light and $t_1 = 45$ ns for convenience. An interesting point is that the fluorescence decay time of the QD array at room temperature increases significantly and approaches that of QD dispersion of 15 ns, as E_{exc} is decreased in the range below ~2.12 eV so that large QDs are preferentially excited. The decay time has a minimum value when E_{exc} is at ~2.25 eV. In this case, small QDs are considered to be preferentially excited because E_{exc} is slightly higher than the fast absorption peak. When E_{exc} is increased in the range above ~2.28 eV, the decay time increases because the fluorescence from large QDs excited through higher energy exciton states contributes as described in Sec. III A.

The fluorescence decay time of the QD array at 80 K shows similar behavior: The fluorescence decay time has its minimum at 2.30 eV and increases as E_{exc} decreases. Although the decay profile of the QD dispersion was essentially temperature independent over the range of 80 to 280 K,[23] the decay times of the QD array at 80 K tend to be longer than those at room temperature. When E_{exc} is further decreased, to 2.16 eV, the decay curves nearly agree with that of the QD dispersion, as shown in Fig. 6(b).

To further characterize the dependence of the fluorescence temporal behavior on E_{exc}, fluorescence decay curves in the low-energy region are plotted in Fig. 7. There, the fluorescence intensities are spectrally integrated in a range below $E_f(0) - \sigma$, where $E_f(0)$ is the average fluorescence photon energy at time 0 and σ is the spectral width (standard deviation) of the

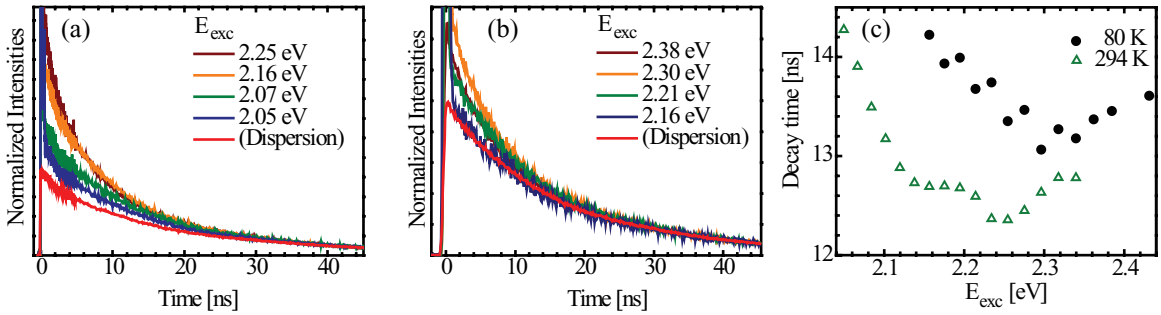

FIG. 6. (Color online) Spectrally integrated fluorescence intensities with various excitation photon energies $E_{\rm exc}$ at (a) room temperature and (b) 80 K. The fluorescence decay curve of QD dispersion is also shown for comparison. The intensities are normalized at 45 ns because contamination of the excitation light appears at the initial stage. (c) Decay time of the spectrally integrated fluorescence intensities of the QD array at room temperature (open triangles) and 80 K (filled circles) as a function of $E_{\rm exc}$.

QD dispersion. At room temperature, decay curves in the low-energy region depend slightly on $E_{\rm exc}$, as shown in Fig. 7(a). In contrast, at 80 K, the temporal behavior of fluorescence intensity in the low-energy region depends strongly on $E_{\rm exc}$, as shown in Fig. 7(b). The initial rise appears clearly for large $E_{\rm exc}$. However, this initial rise is reduced as $E_{\rm exc}$ decreases, and the decay curve almost agrees with that of the QD dispersion when $E_{\rm exc}$ is further reduced, to 2.18 eV.

IV. NUMERICAL SIMULATION AND DISCUSSION

As highlighted above, we have found interesting results concerning the dependence of the time- and spectrally resolved fluorescence intensities of the QD array on the excitation photon energy.

(1) When the excitation photon energy $E_{\rm exc}$ is higher than the band edge, high-energy QDs are selectively excited and the average fluorescence photon energy $E_{\rm fluo}$ is red-shifted with time. The magnitude of the red shift decreases as $E_{\rm exc}$ decreases. When $E_{\rm exc}$ is further decreased, to 2.05 eV, $E_{\rm fluo}$ initially increases with time at room temperature. In contrast, at low temperatures, $E_{\rm fluo}$ monotonically decreases or remains constant even at small $E_{\rm exc}$ values.

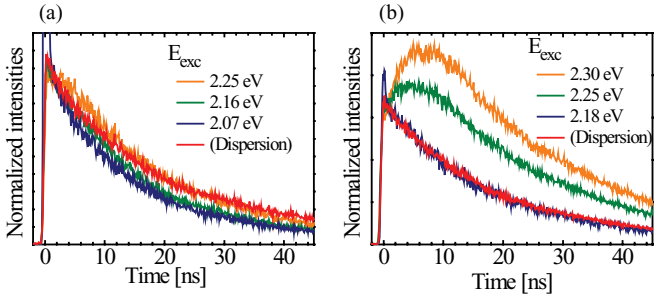

FIG. 7. (Color online) Fluorescence decay curves (low-energy region) with various values of $E_{\rm exc}$ at (a) room temperature and (b) 80 K. The fluorescence decay curve of QD dispersion is also shown. The intensities are normalized at 0.7 ns. The fluorescence intensities are spectrally integrated in a range below $E_f(0) - \sigma$, where $E_f(0)$ is the average fluorescence photon energy at time 0 and σ is the spectral width (standard deviation) of the QD dispersion.

(2) The decay time of spectrally integrated fluorescence intensity is generally shorter than that of the QD dispersion. However, it increases and approaches that of the QD dispersion as $E_{\rm exc}$ is decreased.

(3) At low temperature and for large $E_{\rm exc}$, the initial rise appears in the low-energy region of the fluorescence spectrum. This initial rise is reduced as $E_{\rm exc}$ decreases. When $E_{\rm exc}$ is further reduced, to 2.18 eV, the decay curve agrees with that of the QD dispersion.

To explain these experimental findings and shed light on the exciton dynamics, we performed numerical calculations using a model of a coupled QD array. The governing equations for the exciton dynamics are given by[23]

$$\frac{d\rho_n}{dt} = \sum_{m\neq n} W_{nm}\rho_m - (W_{nn} + 1/\tau_{n,R} + 1/\tau_{n,N})\rho_n, \qquad (2)$$

where $\rho_n = w_n|n\rangle\langle n|$ is the nth diagonal element of the reduced density matrix of the system with probability w_n in the mixed state, and $\tau_{n,R}$ and $\tau_{n,N}$ denote, respectively, the radiative and nonradiative decay times for the nth eigenstate. In the limit of weak electronic coupling between QDs, the nth eigenstate is given by

$$|n\rangle = |e_n\rangle \prod_{l\neq n}^{N} |g_l\rangle, \qquad (3)$$

where $|e_n\rangle$ and $|g_l\rangle$ are the excited and ground electronic states of the nth and lth QD, respectively. Here N is the total number of QDs in the system. Equation (3) means that only the nth QD is in its excited state, while the others are in their ground states. In this case, the transition rate from level $|m\rangle$ to level $|n\rangle$, W_{nm}, can be written as the Förster expression,[40,41]

$$W_{nm} = \frac{|C_{nm}|^2}{2\pi\hbar^2}\int_{-\infty}^{\infty} d\omega F_m(\omega)A_n(\omega), \qquad (4)$$

where C_{nm} is a coupling constant between the nth and the mth QDs related to Coulomb dipole-dipole coupling. The transition rate from the nth QD to the neighboring QDs is defined by $W_{nn} = \sum_{l\neq n} W_{ln}$. $F_m(\omega)$ and $A_n(\omega)$ are the fluorescence spectrum of the mth QD and the absorption spectrum of the nth QD, respectively. In the high-temperature limit and when the nuclear dynamics of a QD crystal is sufficiently slow compared

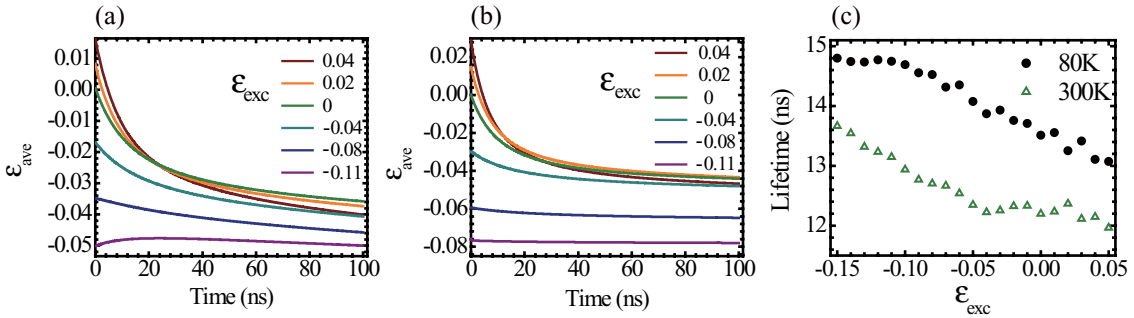

FIG. 8. (Color online) Time traces of the average exciton energy ϵ_{ave} with various excitation photon energies ϵ_{exc} at (a) 300 K and (b) 80 K. (c) Decay time as a function of ϵ_{exc} at 300 K (open triangles) and 80 K (filled circles).

with the magnitude of the fluctuation (slow-modulation limit), the fluorescence and absorption line shapes are expressed in terms of Gaussian profiles:[42]

$$F_m(\omega) = \frac{\hbar}{\sqrt{2\pi}\sigma_h}\exp\left[-(\hbar\omega - \epsilon_m + 2\Delta)^2/2\sigma_h^2\right], \quad (5)$$

$$A_n(\omega) = \frac{\hbar}{\sqrt{2\pi}\sigma_h}\exp\left[-(\hbar\omega - \epsilon_n)^2/2\sigma_h^2\right], \quad (6)$$

where ϵ_m is the exciton energy level of the mth QD and Δ is the lattice reorganization energy with the Stokes shift given by 2Δ. Furthermore, in the high-temperature and slow-modulation limits, the line width of the individual QD is directly related to the Stokes shift and temperature through the relation $\sigma_h^2 = 2\Delta k_B T$.[42,43]

We assume a hexagonal 2D lattice of 50×50 sites. Only nearest-neighbor coupling is taken into account, for simplicity. Furthermore, we do not consider the orientational factor between dipoles and assume the same coupling strength for adjacent QD pairs with $C_{nm} = 1.5 \times 10^{-4}$ eV. The inhomogeneous broadening of the energy level ϵ_n related to the size distribution is given by a Gaussian with $\sigma_{ih} = 33$ (meV), with an average value of 0. The Stokes shift is set to be $2\Delta = 57$ (meV).

We incorporate dark QDs that exhibit fast nonradiative decay in the array in view of the fact that the fluorescence intensity of a blinking QD is generally correlated with its decay time.[37–39] For example, Rosen *et al.* observed, by single-molecule spectroscopy techniques, that the fluorescence decay time of an off-state CdSe/CdZnS QD is 250 ps, which is much faster than that of an on-state QD, which has a decay time of tens of nanoseconds.[38] In the numerical calculation, we assume that $\tau_{n,N} = \infty$ for the bright QD and $\tau_{n,N} = 0.1$ (ns) for the dark QD. The ratio of the number of dark QDs to the number of all QDs γ is set to be 0.2. The bright and dark QDs are randomly distributed in the lattice. The radiative decay rate is set to be $\tau_{n,R} = 15$ (ns) for all the QDs, irrespective of n.

In the above parameter set, values of σ_{ih}, 2Δ, and $\tau_{n,R}$ come from the experimental results, and $\tau_{n,N}$ for the dark QD is given roughly according to the literature.[38] On the other hand, C_{nm} and γ are given to fit the experimental results.

The excitation probability of each QD is given according to the absorption spectrum of Eq. (6). To examine the effect of selective excitation on fluorescence intensity, the excitation photon energy is varied while holding the other parameters constant. The fluorescence intensity is assumed to be proportional to the population of the excited states. In this case, the spectrally integrated fluorescence intensity is simply given by $I(t) \propto \langle \sum_n \rho_n \rangle$. Here $\langle \cdots \rangle$ denotes the average over a set of excited states.

Figures 8(a) and 8(b) show time traces of the average exciton energy,

$$\epsilon_{ave}(t) = \left\langle \sum_n \rho_n(t)\epsilon_n \right\rangle \Big/ \left\langle \sum_n \rho_n(t) \right\rangle,$$

with various excitation photon energies ϵ_{exc} at 300 and 80 K, respectively. For large ϵ_{exc}, during the initial stages, ϵ_{ave} decreases significantly, and then the rate of the red shift decreases with time. The magnitude of the red shift decreases as ϵ_{exc} decreases. This fact suggests that excitons preferentially transfer from higher energy QDs. It is noteworthy that, at room temperature, ϵ_{ave} increases slightly during the initial stage when ϵ_{exc} is reduced to -0.11. This increase in ϵ_{ave} can be attributed to exciton transfer from a lower to a higher energy QD. In contrast, ϵ_{ave} monotonically decreases or remains constant at 80 K even for small ϵ_{exc}. These trends qualitatively agree with the experimental results shown in Figs. 3 and 5.

Figure 8(c) shows the fluorescence decay time as a function of ϵ_{exc}. The decay time at 300 K tends to be shorter than that at 80 K. The decay time increases and apparently approaches the value of the radiative decay time of 15 ns as ϵ_{exc} decreases. This is consistent with the experimental result shown in Fig. 6(c). In the experiment, when E_{exc} is increased above $\sim$2.28 eV, the decay time increases because the contribution of the fluorescence from large QDs excited through higher energy levels becomes dominant, as described in Sec. III A. On the other hand, in the numerical calculations, we do not consider the excitation to higher exciton energy levels, for simplicity. Therefore, the decay time does not reach a minimum and monotonically decreases as ϵ_{exc} increases.

Figure 9 shows the fluorescence decay curves in the low-energy region at $-2\Delta - \sigma_{ih}$ with various values of ϵ_{exc}. At 80 K, an initial rise clearly appears for positive ϵ_{exc}. This rise is reduced with decreasing ϵ_{exc}. In contrast, the decay curve at 300 K depends only slightly on ϵ_{exc}, which is also consistent with the experimental result shown in Fig. 7.

To provide further understanding of exciton dynamics, we examine the effect of selective excitation on the hopping length. Figures 10(a) and 10(b) show time traces of the square of the hopping length with various initial energy levels ϵ_{init}.

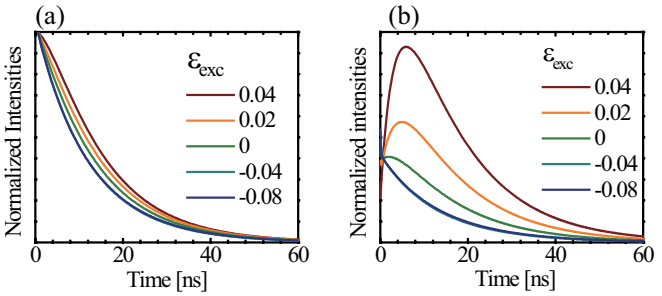

FIG. 9. (Color online) Fluorescence decay curves in the low-energy region ($-2\Delta - \sigma_{ih}$) with various values of excitation photon energy ϵ_{exc} at (a) 300 K and (b) 80 K. The intensities are normalized at 0.7 (ns). The time traces at $\epsilon_{exc} = -0.04$ and -0.08 overlap at both temperatures.

The square of the hopping length at time t is defined by $R(t)^2 = \langle\langle \sum_n \rho_n(t)(\mathbf{r}_n - \mathbf{r}_0)^2\rangle / \langle\sum_n \rho_n(t)\rangle\rangle_e$. Here, $\mathbf{r}_n$ is the position of the nth QD and $\langle\cdots\rangle_e$ is the ensemble average over all trials. Initially, only a single bright QD at $\mathbf{r}_0$ with energy level ϵ_{init} is excited. The interdot distance d is set to be unity. All the results of the numerical calculation are averaged over 100 ensembles of the QD arrays. Also shown in Fig. 10(c) is the square of the average hopping length as a function of ϵ_{init}, which is defined by

$$R^2_{ave} = \left\langle\left\langle \int_0^\infty \sum_n \rho_n(t)(\mathbf{r}_n - \mathbf{r}_0)^2 \right\rangle \Big/ \left\langle \int_0^\infty \sum_n \rho_n(t) \right\rangle\right\rangle_e . \tag{7}$$

We find that $R^2(t)$ (and R^2_{ave}) increases as ϵ_{init} increases, and $R^2(t)$ (and R^2_{ave}) at 300 K tends to be larger than that at 80 K. At 80 K, $R^2(t)$ remains almost 0 for small ϵ_{init}. It is evident that $R^2(t)$ increases monotonically with time, although the slope of $R^2(t)$ decreases with time, especially for large ϵ_{init}. This temporal change in the slope of $R^2(t)$ suggests that the hopping probability decreases with time owing to the thermal relaxation in the system.

On the basis of these findings, the effect of selective excitation on the dynamics of exciton hopping can be explained as follows (see the schematic illustration in Fig. 11):

(1) When an exciton is photogenerated in a high-energy QD, it preferentially transfers to a site of low energy. The exciton is quenched if it reaches a dark QD. Therefore, ϵ_{ave} decreases in time, accompanying a decrease in the fluorescence decay time.

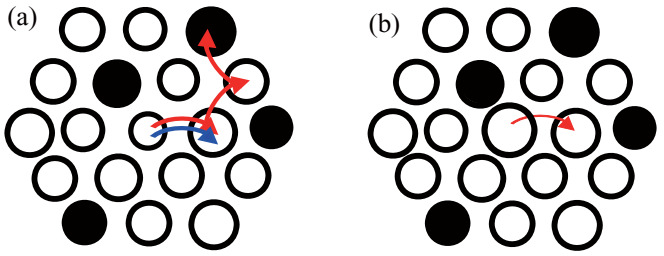

FIG. 11. (Color online) Schematic illustration of the exciton dynamics in the QD array. Open and filled circles in the array correspond to bright and dark QDs, respectively. (a) When an exciton is photoexcited in a high-energy QD, energy transfer occurs preferentially to a low-energy QD. At low temperatures, the exciton is trapped on a local low-energy site after energy transfer occurs, as shown by the bottom-most (blue) arrow. In contrast, at room temperature, the exciton hops repeatedly until it is transferred to a dark QD, where it undergoes nonradiative recombination, as shown by the upper two (red) arrows. (b) When an exciton is photoexcited in a low-energy QD, the exciton tends to be trapped in it. However, at room temperature, there is a non-negligible probability of the exciton transferring from a lower to a higher energy QD.

When the magnitude of the thermal fluctuation is smaller than the site energy distribution at a low temperature, i.e., $\sigma_h \ll \sigma_{ih}$, energy transfer occurs predominantly from a high- to a low-energy QD. Therefore, the exciton is trapped on a local low-energy site after energy transfer occurs. This induces a rise in fluorescence in the low-energy region of the fluorescence spectrum.

In contrast, at room temperature with $\sigma_h \sim \sigma_{ih}$, the exciton can transfer from a low- to a high-energy site via phonon absorption. In this case, exciton energy transfer is expected to occur repeatedly, leading to a large hopping length. This exciton behavior accompanies a significant decrease in the fluorescence decay time because of the high probability of the exciton transferring to the dark QD, followed by decay via nonradiative recombination. In the high-temperature limit, the degree of site selectivity as well as the effect of inhomogeneities is reduced because all QDs can be considered spectrally identical. In this case, the exciton tends not to be trapped on a low-energy site, and thus, the initial rise is reduced in the low-energy region of the fluorescence spectrum.

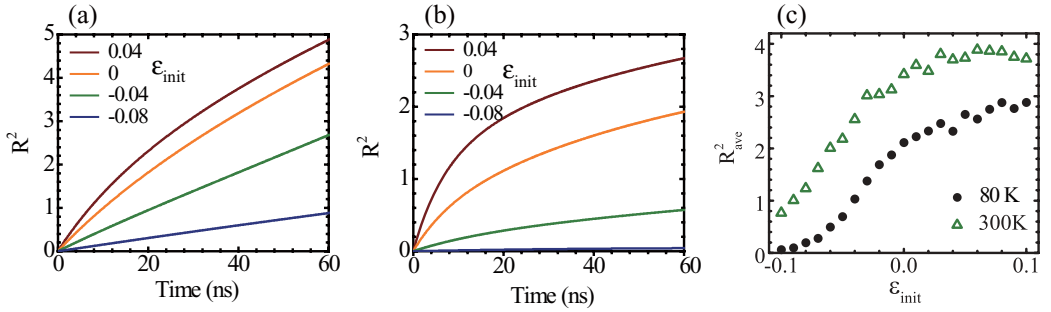

FIG. 10. (Color online) Time traces of the square of the hopping length, R^2, with various initial energy levels ϵ_{init} at (a) 300 K and (b) 80 K. (c) Square of the average hopping length R^2_{ave} as a function of ϵ_{init} at 300 K (open triangles) and 80 K (filled circles).

(2) When an exciton is initially photoexcited in a low-energy QD, it tends to be trapped on it. This corresponds to the fact that the energy transfer rate of Eq. (4) is low when $|\epsilon_{\rm init} - 2\Delta| \gg 2\sigma_{\rm h}$ $(=2\sqrt{2\Delta k_B T})$. In this case, $\epsilon_{\rm ave}$ remains in the low-energy region, and the decay time approaches that of QD dispersion because the exciton tends not to transfer to neighboring dark QDs. However, at room temperature, because there is a non-negligible probability of the exciton transferring from a lower to a higher energy QD, $\epsilon_{\rm ave}$ slightly increases with time. In contrast, at low temperatures, an exciton is trapped predominantly on the initial site, and consequently, the fluorescence decay curve agrees well with that of QD dispersion.

In the theoretical analysis and the numerical calculation, fluorescence and absorption spectra are simply assumed to be a Gaussian. Experimental results are well reproduced by using this model. However, at low temperatures, phonon side bands appear, as shown in Fig. 4. Therefore, it is necessary to incorporate this vibronic transition as well as determine the number of off-state QDs in the ensemble to quantitatively explain the experimental results.

V. CONCLUSION

Site-selective excitation of fluorescence spectra is a powerful tool for studying energy transfer within an ensemble with an inhomogeneous distribution. This method has been applied to measure the exciton energy transfer in CdSe/ZnS QD arrays by varying the excitation photon energy at both room and low temperatures. We have shown that the decrease in the decay time and the dynamic red shift in the fluorescence spectrum are attributable to exciton energy transfer in the inhomogeneous QD ensemble. As the excitation photon energy decreases, the magnitude of the dynamic red shift of the fluorescence spectrum decreases while the fluorescence decay time increases. Numerical calculations are performed by using a model of a coupled QD array including bright and dark QDs, and the calculations agree well with the experiment. From these results, it can be concluded that, when the low-energy end of the QD ensemble is selectively excited, the exciton tends to be trapped in it. In contrast, when high-energy QDs are excited, exciton energy transfer occurs to a site of low energy until it reaches a dark QD followed by nonradiative recombination.

The experimental method and the analysis described in this study provide some general insight and a better understanding, especially toward realizing nanocrystal solar cells. In addition to QDs, they can be applied to various systems such as light-harvesting antennae and conjugated polymer blends, where the hopping exciton is trapped by a quenching molecule. Thus, the present study is expected to provide further understanding of relevant natural systems and facilitate the realization of new optoelectronic devices.

*Corresponding author: miyazaki@ils.uec.ac.jp

[1] N. J. Wu, M. Kamada, A. Natori, and H. Yasunaga, Jpn. J. Appl. Phys. **39**, 4642 (2011).
[2] G. Burkard, D. Loss, and D. P. DiVicenzo, Phys. Rev. B **59**, 2070 (1999).
[3] S. Sangu, K. Kobayashi, A. Shojiguchi, and M. Ohtsu, Phys. Rev. B **69**, 115334 (2004).
[4] I. Gur, N. A. Fromer, and M. L. Geier, Science **310**, 462 (2005).
[5] S. Lu, Z. Lingley, T. Asano, D. Harris, T. Barwicz, S. Guha, and A. Madhukar, Nano Lett. **9**, 4548 (2009).
[6] C. R. Kagan, C. B. Murray, M. Nirmal, and M. G. Bawendi, Phys. Rev. Lett. **76**, 1517 (1996).
[7] C. R. Kagan, C. B. Murray, and M. G. Bawendi, Phys. Rev. B **54**, 8633 (1996).
[8] O. I. Mićić, K. M. Jones, A. Cahill, and A. J. Nozik, J. Phys. Chem. B **102**, 9791 (1998).
[9] S. A. Crooker, J. A. Hollingsworth, S. Tretiak, and V. I. Klimov, Phys. Rev. Lett. **89**, 186802 (2002).
[10] M. Achermann, M. A. Petruska, S. A. Crooker, and V. I. Klimov, J. Phys. Chem. B **107**, 13787 (2003).
[11] T. Franzl, D. S. Koktysh, T. A. Klar, A. L. Rogach, J. Feldmann, and N. Gaponik, Appl. Phys. Lett. **84**, 2904 (2004).
[12] T. Franzl, A. Shavel, A. L. Rogach, N. Gaponik, T. A. Klar, and A. Eychmuller, Small **1**, 392 (2005).
[13] S. F. Wuister, R. Koole, C. M. Donegá, and A. Meijerink, J. Phys. Chem. B **109**, 5504 (2005).
[14] N. Cicek, S. Nizamoglu, T. Ozel, E. Mutlugun, D. U. Karatay, V. Lesnyak, T. Otto, N. Gaponik, A. Eychmüller, and H. V. Demir, Appl. Phys. Lett. **94**, 061105 (2009).
[15] M. Lunz, A. L. Bradley, W. Chen, and Y. K. Guńko, J. Phys. Chem. C **113**, 3084 (2009).
[16] M. Lunz, A. L. Bradley, W. Y. Chen, V. A. Gerard, S. J. Byrne, Y. K. Gun'ko, V. Lesnyak, and N. Gaponik, Phys. Rev. B **81**, 205316 (2010).
[17] M. Lunz, A. L. Bradley, V. A. Gerard, S. J. Byrne, Y. K. Gun'ko, V. Lesnyak, and N. Gaponik, Phys. Rev. B **83**, 115423 (2011).
[18] C. Higgins, M. Lunz, A. L. Bradley, V. A. Gerard, S. Byrne, Y. K. Guńko, V. Lesnyak, and N. Gaponik, Opt. Express **18**, 24486 (2010).
[19] K. Akahane, N. Yamamoto, M. Naruse, T. Kawazoe, T. Yatsui, and M. Ohtsu, Jpn. J. Appl. Phys. **50**, 04DH05 (2011).
[20] F. Shafiei, S. P. Ziama, E. D. Curtis, and R. S. Decca, Phys. Rev. B **84**, 075301 (2011).
[21] A. M. van Oijen, M. Ketelaars, J. Köhler, T. J. Aartsma, and J. Schmidt, Biophys. J. **78**, 1570 (2000).
[22] A. Damjanović, I. Kosztin, U. Kleinekathöfer, and K. Schulten, Phys. Rev. E **65**, 031919 (2002).
[23] J. Miyazaki and S. Kinoshita, J. Phys. Soc. Jpn **81**, 074708 (2012).
[24] R. Berera, C. Herrero, I. H. M. van Stokkum, M. Vengris, G. Kodis, R. E. Palacios, H. van Amerongen, R. van Grondelle, D. Gust, T. A. Moore, A. L. Moore, and J. T. M. Kennis, Publ. Natl. Acad. Sci. USA **103**, 5343 (2006).
[25] R. Berera, I. H. M. van Stokkum, S. d'Haene, J. T. M. Kennis, and R. van Grondelle, Biophys. J. **96**, 2261 (2009).
[26] N. E. Holt, D. Zigmantas, L. Valkunas, X. P. Li, K. K. Niyogi, and G. R. Fleming, Science **21**, 433 (2005).

[27]D. F. O'Briena, M. A. Baldo, M. E. Thompson, and S. R. Forrest, Appl. Phys. Lett. **74**, 442 (1999).
[28]M. Achermann, M. A. Petruska, D. D. Koleske, M. H. Crawford, and V. I. Klimov, Nano Lett. **6**, 1396 (2006).
[29]J. Dexpert-Ghys, M. Faucher, and P. Caro, Phys. Rev. B **23**, 607 (1981).
[30]L. M. Herz, C. Silva, A. C. Grimsdale, K. Mullen, and R. T. Phillips, Phys. Rev. B **70**, 165207 (2004).
[31]S. Westenhoff, W. J. D. Beenken, R. H. Friend, N. C. Greenham, A. Yartsev, and V. Sundstrom, Phys. Rev. Lett. **97**, 166804 (2006).
[32]H.-C. Chiou, S. Lin, and R. E. Blankenship, J. Phys. Chem. **101**, 4136 (1997).
[33]M. Nirmal, B. O. Dabbousi, M. G. Bawendi, J. J. Macklin, J. K. Trautman, T. D. Harris, and L. E. Brus, Nature **383**, 802 (1996).
[34]A. L. Efros and M. Rosen, Phys. Rev. Lett. **78**, 1110 (1997).
[35]M. Ye and P. C. Searson, Phys. Rev. B **84**, 125317 (2011).
[36]M. Califano, J. Phys. Chem. C **115**, 18051 (2011).
[37]B. R. Fisher, H.-J. Eisler, N. E. Stott, and M. G. Bawendi, J. Phys. Chem. B **108**, 143 (2004).
[38]S. Rosen, O. Schwartz, and D. Oron, Phys. Rev. Lett. **104**, 157404 (2010).
[39]C. Galland, Y. Ghosh, A. Steinbrück, M. Sykora, J. A. Hollingsworth, V. I. Klimov, and H. Htoon, Nature **479**, 203 (2011).
[40]M. Yang and G. R. Fleming, Chem. Phys. **275**, 355 (2002).
[41]A. Ishizaki and G. R. Fleming, J. Chem. Phys. **130**, 234111 (2009).
[42]S. Mukamel, *Principles of Nonlinear Optical Spectroscopy* (Oxford University Press, New York, 1995).
[43]G. D. Scholes and D. L. Andrews, Phys. Rev. B **72**, 125331 (2005).